Potential Energy Surface of the $O(^1D) + N_2O \rightarrow 2NO$, $O_2 + N_2$ Reactions

I. Last,* A. Aguilar, R. Sayós, M. González, and M. Gilibert

Departament de Química Física, Universitat de Barcelona, Martí i Franquès 1, 08028 Barcelona, Spain

Received: June 20, 1996; In Final Form: October 7, 1996[⊗]

Using the Møller−Plesset method the *ab initio* N_2O_2 potential energy surface (PES) is calculated in order to study the exothermic singlet state reaction channels $O(^1D) + N_2O \rightarrow 2NO$, $O_2(a\ ^1\Delta_g) + N_2$. According to the results of the calculation, the $O(^1D) + N_2O \rightarrow 2NO$ channel PES demonstrates the main energy release in the entrance valley. In this channel a wide interval of $\angle O(^1D)NN$ approach angles around the collinear configuration is easily accessible, but the minimum energy approach is not collinear. The $O(^1D) + N_2O \rightarrow O_2(a\ ^1\Delta_g) + N_2$ channel is strongly noncollinear, as the minimum energy $\angle O(^1D)ON$ approach angle is close to 90°. The main energy release of this channel takes place in the exit valley. The results of the *ab initio* calculations have been used to construct an analytical model potential that describes roughly the main features of the N_2O_2 PES and can be used in the dynamical studies of both $O(^1D) + N_2O$ reaction channels.

1. Introduction

The reaction of the ground state oxygen atom $O(^3P)$ with N_2O displays a large activation energy and consequently is not of much interest.[1] In contrast to the $O(^3P)$ case the singlet state oxygen atom $O(^1D)$ reacts with the N_2O molecule either without any barrier or with a small one.[2,3] Theoretically, there are five $O(^1D) + N_2O$ exothermic reaction channels, but only two of them, namely,

$$O(^1D) + N_2O \rightarrow 2NO \qquad (1)$$

$$O(^1D) + N_2O \rightarrow O_2 + N_2 \qquad (2)$$

are of importance, as other three channels contribute a total of a few percents only.[4] The exothermicities of reaction channels 1 and 2, ΔH_0, are high, 3.53[5] and 5.4 eV,[6] respectively.

In the experimental studies of the reactions (1) and (2) the excited $O(^1D)$ atoms are mostly produced by UV photodissociation of the N_2O molecules.[7−9] The free $O(^1D)$ atoms collide with the nondissociated N_2O molecules and react with them with a near unit efficiency.[1,10] Most attention in the experimental studies has been paid to the reaction (1),[10−16] as the product of this reaction, NO, is a much easier object for spectroscopic analysis than the homonuclear O_2 and N_2 molecules, the reaction (2) products. The experimental studies of the reaction (2) are restricted mainly to the problem of the reaction branching values.[1,4,6,17]

The final products of both reaction channels are ground state molecules. However, the direct formation of the triplet ground state oxygen molecule in reaction channel (2) is spin forbidden, as both reaction species are in a singlet state. Theoretically the nonadiabatic transition may be responsible for the O_2 ($X\ ^3\Sigma_g^-$) formation, but the probability of such a transition is expected to be low. It is much more realistic to suggest that the formation of the final product ground state molecules O_2 ($X\ ^3\Sigma_g^-$) involves two steps. The first one is the reaction channel that gives rise to electronically excited single state O_2 molecules, either $O_2(a\ ^1\Delta_g)$ or $O_2(b\ ^1\Sigma_g^+)$.[1,2] This reaction channel is followed by the deactivation of the excited O_2 molecules by collisions, most probably, since the radiative $O_2(a\ ^1\Delta_g)$ deactivation time is long, about 1 h.[4] The deactivation of $O_2(b\ ^1\Sigma_g^+)$ to $O_2(a\ ^1\Delta_g)$ is very rapid.[18] The formation of the excited $O_2(a\ ^1\Delta_g)$ molecules in the direct reaction

$$O(^1D) + N_2O(X\ \Sigma_g^+) \rightarrow O_2(a\ ^1\Delta_g) + N_2(X\ ^1\Sigma_g^+) \qquad (3)$$

or by the $O_2(b\ ^1\Sigma_g^+)$ deactivation was confirmed experimentally by detecting the energy transfer from $O_2(a\ ^1\Delta_g)$ to Tl atoms.[19] Taking into account the $O_2(a\ ^1\Delta_g)$ dissociation energy of $D_0 = 4.138$ eV,[20] one obtains the reaction (3) exothermicity of $H_0 = -4.386$ eV.

To study theoretically the reactions (1) and (3), one needs the potential energy surface (PES) of the N_2O_2 system. The only known *ab initio* PES used for the $O(^1D) + N_2O$ reaction study was performed at a low-accuracy Hartree−Fock (HF) level and was restricted to the case of the $O(^1D)$ interaction with the N_2O molecule of a frozen geometry.[15] The results of the *ab initio* calculation of the $(NO)_2$ dimer[21] and metastable N_2O_2 isomers (performed in either the Møller−Plesset (MP) or CI approach)[22,23] are also of some limited use for the reaction PES description. A semiempirical LEPS type PES of the $O(^1D) + NNO$ interaction was introduced recently in order to perform trajectory calculation of the reaction (1).[5] This PES, however, cannot be considered as a realistic one, due to an arbitrary choice of the Sato parameters.[5]

The main goal of the present work is the *ab initio* calculation of the N_2O_2 PES and especially the minimum energy paths of the reaction channels (1) and (3). It is practically impossible to produce the PES of such a complicated reactive system by using very accurate methods like CI. However, since the channels under consideration are highly exothermic and are not expected to have any potential barriers, some less accurate *ab initio* calculations of the system will be of obvious interest. In the present work the calculation has been performed by using the MP perturbation approach. We constructed also an analytical model PES that fits roughly the main features of the *ab initio* PES. This model potential will be used in a dynamical study of the $O(^1D) + N_2O$ reaction channels.

2. *Ab Initio* Calculation of the N_2O_2 System

The *ab initio* calculations of the N_2O_2 system have been performed by the Møller−Plesset perturbation method with unrestricted Hartree−Fock (UMP) carried out by using the

* Corresponding author. Permanent address: Soreq NRC, Yavne 81800, Israel.

[⊗] Abstract published in *Advance ACS Abstracts,* January 15, 1997.

S1089-5639(96)01847-6 CCC: $14.00

TABLE 1: *Ab Initio* (UHF, UMP2, UMP4) Energies, *E* (in au), of Atoms N and O and the $O(^1D)$ Excitation Energy; *E (in eV); The Experimental Value $E^* = 1.968$ eV**

	$N(^4S)$ $-E-54$	$O(^3P)$ $-E-74$	$O(^1D)$ $-E-74$	$O(^1D)$ E^*
UHF	0.397 98	0.805 89	0.678 10	3.477
UMP2	0.502 51	0.951 46	0.843 04	2.950
UMP4	0.520 54	0.968 77	0.867 56	2.754

GAUSSIAN 92 package of programs[24] and an IBM RISC/6000 3 AT workstation. Most results were obtained at the second-order (UMP2) level, but for some configuration points, mainly in the collinear geometry, the fourth-order (UMP4) level was applied as well. The standard Gaussian basis set 6-311G(2d) was used.

We exclude from our consideration the reaction channels with the excited state $O_2(b\ ^1\Sigma_g^+)$ as a product. Having excluded also the nonadiabatic transitions to a triplet state, we are left with the reaction channels (1) and (3). The three-dimensional (3D) PESs of these channels were calculated for the singlet state, which is asymptotically connected to the reactants $O(^1D) + N_2O$ and the products NO + NO (with opposite spins) and $O_2(a\ ^1\Delta_g)$ + N_2 (the molecules N_2O, NO, and N_2 are in their ground electronic state). The main purpose of the N_2O_2 PES calculation was the determination of the minimum energy paths for both reaction channels, (1) and (3). The minimum energy paths were found by both UMP2 and UMP4 calculation levels in the case of collinear geometry and by UMP2 calculation level in the 3D case. To provide some useful supplementary information about the 3D PES, a number of configurations outside the minimum energy paths were considered as well. The calculations were restricted to the 3D PESs, which in the planar geometry become $^1A'$ symmetric. In addition to the singlet state calculations we also performed, on a small scale, the calculations of a triplet PES which is asymptotic to the ground state reactants and channel (2) products.

Prior to calculating the N_2O_2 PES in the interaction region we need to perform the calculations of the atoms $N(^4S)$, $O(^3P)$, and $O(^1D)$ and molecules $NO(X\ ^2\Pi)$, $N_2(X\ ^1\Sigma_g^+)$, $O_2(a\ ^1\Delta_g)$, and $N_2O(X\ ^1\Sigma_g^+)$, which are involved in the reaction channels (1) and (3). The results of these calculations are presented in Tables 1−3 for three accuracy levels, namely, the unrestricted Hartree−Fock (UHF) and the Møller−Plesset UMP2 and UMP4. The most serious problem is presented by the single state $O(^1D)$ atom, whose wave function is known to be described by the superposition of at least two configurations, whereas the MP approach is based on the one-configuration HF presentation.[29] In the MP approach, however, the interelectron correlation is taken partly into account so that the effect of the configuration interaction is incorporated in some way into the system energy. It is well demonstrated by the $O(^1D)$ excitation energy *E**, which is monotonously decreasing in the accuracy level sequence UHF−UMP2−UMP4 toward the experimental value of $E^* = 1.968$ eV. The UMP4 *E** value is roughly halfway between the UHF and the experimental values.

The molecular dissociation energies D_e are not changing monotonously with the accuracy level, so that UMP2 D_e values are closer to the experimental D_e than those obtained at the UMP4 level (Tables 2 and 3). These results of the UHF calculation are extremely poor: dissociation energies make up not more than 50% of the empirical values. In the $O_2(a\ ^1\Delta_g)$ case the UHF calculation provides even a negative D_e.

The data presented in Tables 1−3 allow the calculation of the reaction (1) and (3) exoergicity, ΔD_e, which is determined as the difference between the reactant and product energies for fixed equilibrium geometries. The ΔD_e values, both *ab initio* and empirical, are presented in Table 4. The UMP4 ΔD_e values are closer to the empirical values than those of the UMP2 level.

It is important to note that the molecular results obtained by the UMP2 calculation do not differ much from the corresponding UMP4 values. For example, the UMP2 exoergicities, ΔD_e, differ from the more accurate UMP4 values by only ∼0.1−1.3 eV (Table 4).

3. Collinear Geometry

Before considering the general case of a three-dimensional (3D) N_2O_2 system, we shall treat the collinear ONNO and OONN PESs, which describe the reaction channels (1) and (3), respectively. The collinear PESs were calculated by using both UMP2 and UMP4 accuracy levels. Comparing the UMP2 and UMP4 results, one can estimate the accuracy of the UMP2 level.

3.1. $O(^1D) + N_2O \rightarrow 2NO$ Collinear Reaction. The collinear reaction (1) is described by the PES of the ONNO system in the singlet $^1\Sigma^+$ state. The minimum energy path of this reaction was found at the UMP4 level. According to the results of the calculation (Figure 1) the $^1\Sigma^+$ PES has a relatively deep local minimum at the symmetrical geometry $R_{ON} = R_{NO} = 1.235$ Å, $R_{NN} = 1.157$ Å (Table 5). The minimum energy points lies 3.294 eV below the reactant $O(^1D)$ + NNO energy and 0.554 eV higher than the product 2NO energy. In Figure 1 the minimum energy point divides the entrance (on left) and exit (on right) valleys. The local PES minimum is separated from the products by a saddle point located approximately at $R_{NN} = 1.67$ Å. The saddle point lies about 1.94 eV over the minimum point, but some 1.35 eV below the reactant level (Table 5), so that it is energetically accessible and does not prevent the reaction.

In the entrance valley ($O(^1D)$−N distance as the reaction coordinate) the NN and NO distances of the NNO molecule are slightly affected by the approaching oxygen atom. Only in the vicinity of the minimum point does the NN distance begin to increase noticeably. In the exit valley (N−N distance as the reaction coordinate) the system is symmetric along the minimum energy path ($R_{ON} = R_{NO}$).

To estimate the accuracy of the UMP2 calculation, we found at this level the PES local minimum and saddle point (Table 5). The UMP2 minimum lies only 0.33 eV lower than the UMP4 one. The differences between the UMP2 and UMP4 interatomic distances are also small, not more than 0.03 Å. The UMP2 saddle point lies 3.14 eV over the minimum compared to the corresponding UMP4 value of 1.94 eV. The UMP2 accuracy of the saddle point calculation is most probably

TABLE 2: *Ab Initio* and Experimental Interatomic Distances, *R* (in Å), Total Energies (in au), and Dissociation Energies, D_e (in eV), of Diatomic Molecules Involved

	$NO(X^2\Pi)$			$N_2(X\ ^1\Sigma_g^+)$			$O_2(a\ ^1\Delta_g)$		
	R	$-E-129$	D_e	*R*	$-E-108$	D_e	*R*	$-E-149$	D_e
UHF	1.116	0.287 50	2.276	1.066	0.978 24	4.960	1.157	0.580 40	−0.854
UMP2	1.136	0.686 36	6.323	1.112	1.358 89	9.629	1.257	1.049 08	3.977
UMP4	1.141	0.712 20	6.065	1.112	1.381 22	9.255	1.255	1.071 18	3.636
exptl	1.151[a]		6.614[b]	1.098[c]		9.905[c]	1.216[d]		4.231[d]

[a] References 25. [b] Estimated from ref 25. [c] Reference 26. [d] Reference 20.

TABLE 3: *Ab Initio* and Experimental Interatomic Distances, *R* (in Å), Total Energies (in au), and $N_2O \rightarrow N_2 + O(^1D)$, $2N + O(^3P)$ Dissociation Energies, D_e (in eV), of the N_2O Molecule (Linear Equilibrium Geometry)

	R			D_e	
	NN	NO	$-E$-183	$N_2 + O(^1D)$	$2N + O(^3P)$
UHF	1.082	1.172	0.737 81	2.217	3.700
UMP2	1.156	1.182	1.383 72	4.947	11.625
UMP4	1.158	1.196	1.415 42	4.534	11.035
exptl	1.127[a]	1.185[a]		3.76[b]	11.70[b]

[a] Reference 27. [b] Reference 28.

TABLE 4: *Ab Initio* and Experimental Exoergicity, ΔD_e (in eV), of the Reaction Channels (a) $O(^1D) + N_2O \rightarrow 2NO$ and (b) $O(^1D) + N_2O \rightarrow O_2$ ($a\ ^1\Delta_g$) $+ N_2$; The Experimental ΔD_e Was Calculated by Using the Data of Tables 2 and 3

	reaction	
	(a)	(b)
UHF	4.239	3.884
UMP2	3.971	4.931
UMP4	3.849	4.610
exptl	3.499	4.407

affected by an avoiding crossing, which is expected in the saddle point region. The UMP2 saddle point geometry does not differs much from that of the UMP4 calculation.

3.2. $O(^1D) + N_2O \rightarrow O_2(a\ ^1\Delta_g) + N_2$ Collinear Reaction. The collinear reaction (3) is described by the PES of the OONN system in the $^1\Delta$ state. Like in the previous case the minimum energy path of this reaction was found by the UMP4 level calculation.

The shape of the minimum reaction path is simple (Figure 2). In the entrance valley the potential energy increases smoothly, reaching at $R_{OO} \approx 1.55$ Å the saddle point with a potential energy of roughly 2.6 eV (Table 5). The saddle point in Figure 2 divides the entrance (on left) and exit (on right) valleys. In the exit valley the potential energy is decreasing steeply with the reaction coordiante R_{ON}. The NN distance is not changing much in both entrance and exit valleys, whereas the ON distance is increasing sharply when the oxygen atom approaches the ONN molecule. The UMP2 calculation provides a higher barrier than the UMP4 one (Table 5). However the difference is not big, only about 0.5 eV.

The comparison of the UMP2 and UMP4 results obtained for the collinear ONNO and OONN systems (Table 5), as well as for the component molecules (Tables 2 and 3) and exoergicities (Table 4), shows that the UMP4 level mostly provides results not much different from the UMP2 level results. Taking this into account, we decided to produce the 3D PESs by the much less time consuming UMP2 calculation.

4. Three-Dimensional (3D) Geometry

4.1. $O(^1D) + N_2O \rightarrow 2NO$ Reaction. The reaction channel (1) takes place when the singlet state oxygen atom approaches the terminal N atom of the N_2O molecule (Figure 3a). The minimum reaction path of this reaction channel is shown in Figure 4.

The MP treatment of this reaction presents a serious problem when the exit chanel is considered. In the interaction region of this channel, as well as in the entrance channel, the molecular orbitals (MOs) are generally delocalized between all four atoms, and in particular, they follow the system symmetry when the exit channel ONNO geometry becomes symmetrical. On the contrary, in the asymptotic ON + NO region of two separated NO molecules the ground state MOs are localized on the NO fragments without any relation to the system symmetry. To overcome this problem, we considered separately the main (interaction) region ($R_{NN} \leq 2.0$ Å in Figure 4) and the ON + NO asymptotic region ($R_{NN} \geq 2.2$ Å in Figure 4). In the asymptotic region the MOs are introduced in such a way that half of them are localized mainly on the ON fragment, whereas

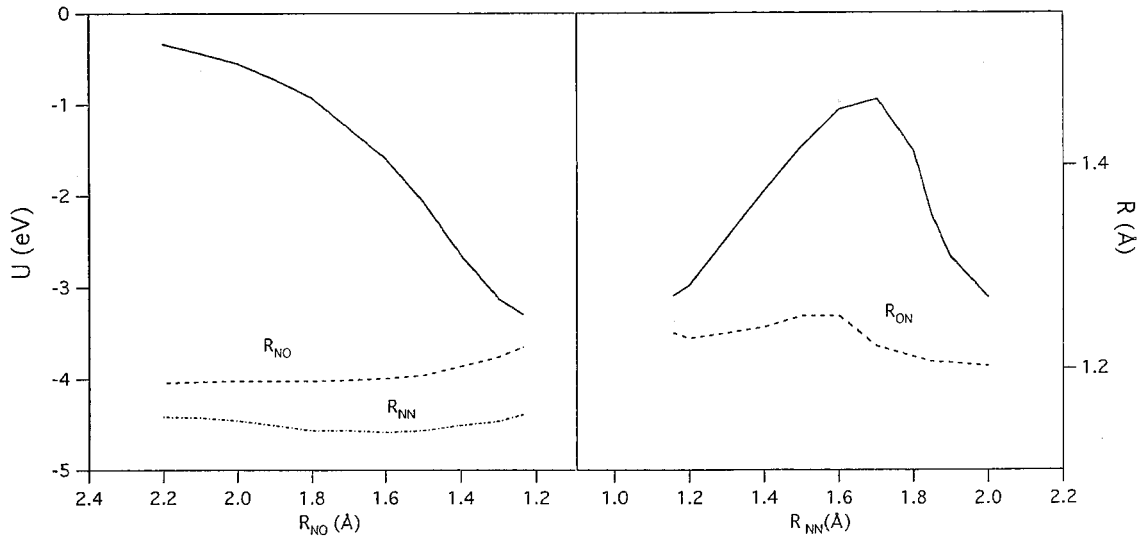

Figure 1. Collinear minimum energy path of the reaction $O(^1D) + NNO \rightarrow ON + NO$. Solid line, potential; broken lines, interatomic distances.

TABLE 5: Local Minimum and Saddle Point Properties of the Collinear ONNO and OONN PESs[a]

	ONNO ($^1\Sigma^+$ state)						OONN ($^1\Delta$ state)			
	minimum			saddle point			saddle point			
	R_{ON}	R_{NN}	U	R_{ON}	R_{NN}	U	R_{OO}	R_{ON}	R_{NN}	U
UMP2	1.215	1.150	−3.613	1.24	1.60	−0.47	1.65	1.30	1.14	3.08
UMP4	1.235	1.157	−3.294	1.22	1.67	−1.35	1.55	1.30	1.15	2.60

[a] The ONNO geometry is symmetrical ($D_{\infty h}$ symmetry) with $R_{NO} = R_{ON}$. Distances *R* are in Å; potential energy *U* is in eV. The reactant $O(^1D) + N_2O$ energy is accepted as the *U* reference level.

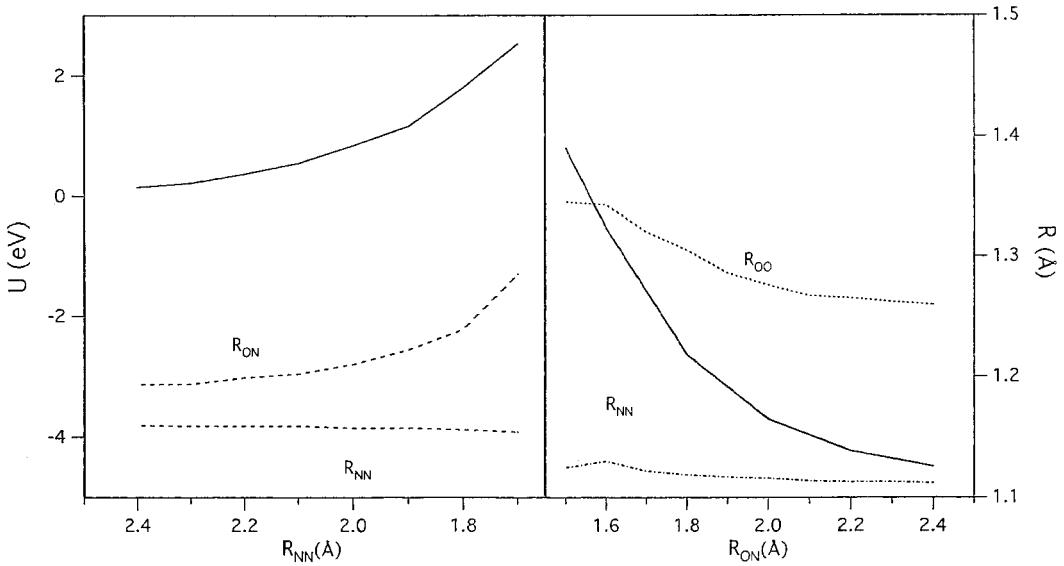

Figure 2. Collinear minimum energy path of the reaction O(^{1}D) + ONN → O_2(a $^1\Delta_g$) + N_2. For notations see Figure 1.

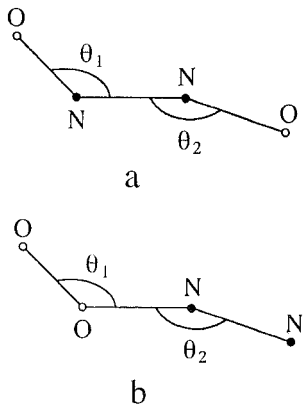

Figure 3. The geometry of (a) ONNO and (b) OONN configurations.

the other half are localized mainly on the NO fragment. The minimum energy paths of these two regions match each other reasonably well (Figure 4a).

In the entrance valley the minimum energy path of the reaction channel (1) (Figure 4a) demonstrates a steep descent to a potential minimum point which is separated from the products by a saddle point. The reaction, however, does not have any potential barrier, as the saddle point lies much below the reactant level. The 3D minimum energy path of the reaction channel (1) was found to lie in a planar geometry and to belong to the ^{1}A′ state. The minimum energy path geometry is shown in Figure 4b. According to Figure 4b, the 3D minimum energy path is far from being collinear.

The properties of the particular points of the minimum energy path, namely, the minimum and the saddle point, are presented in Table 6. The minimum lies 4.16 eV below the reactant level. The ONNO minimum geometry is symmetric, like in the collinear case, with a trans arrangement of the O atoms. The ONNO minimum has a compact geometry with the ON and NN distances not much larger than in the free NO and NN molecules, respectively. The ∠ONN and ∠NNO angles are close to 45°. The saddle point is located approximately at R_{NN} = 1.6 Å, and it lies ∼0.56 eV above the potential minimum point. When the ∠ONN angle deviates from its saddle point value, the potential increases moderately, about 1 eV in the wide angle ∠ONN interval of 85−175° (Figure 5). It follows that the saddle point is widely open. The potential begins to increase sharply for ∠ONN < 85°, which proves that the forces between the O(^{1}D) and the central N atom are repulsive.

Since the system enters the ONNO potential minimum region with a high kinetic energy of about 4 eV, it will pass most probably the widely open saddle point without delay on its way to the products. A cautious conclusion can be made that the ONNO minimum energy region cannot be considered as a long living complex of the reaction (1), opposite of the suggestion made in refs 10 and 11. Due to the deep well, the system releases the overwhelming part of its exoergicity in the entrance valley, colliding with the terminal N atom at a high kinetic energy, which makes a stripping mechanism of the reaction more favorable.[5,13]

According to our results (Table 6), the potential minimum point lies lower than the product 2NO level so that the energy of the ONNO → 2NO dissociation is positive, D_e = 0.19 eV. To determine the D_0 dissociation energy, we need to know the ONNO zero vibrational energy. The vibrational frequencies of the ONNO in-plane deformations are presented in Table 6. Numerical instabilities found in the calculation of the out-of-plane deformations, which were caused probably by a mixture of different electronic configurations, prevent obtaining a realistic estimation of the corresponding UMP2 frequency. We accepted for this out-of-plane frequency, which is expected to be small, the UHF value. The ONNO zero vibrational energy was found to be equal roughly to 0.50 eV. Taking into account the difference between the zero vibrational energy of the ONNO minimum (0.50 eV) and the product NO molecules (0.42 eV), one obtains D_0 = 0.11 eV. The positive dissociation energy D_0 indicates the existence of a stable although very weak bound ONNO complex. However, the accuracy of the present calculation is too low to make a definite conclusion about the existence of such a complex. It can be demonstrated in particular by the following example: if one takes the zero vibrational energy of two NO molecules equal to the experimental value of 0.23 eV (instead of the calculated value of 0.42 eV), the ONNO complex will become metastable (D_0 negative). It is worth noting also that, according to the collinear geometry results (see subsection 3.1), the UMP2 level calculation is expected to overestiamte the ONNO potential minimum depth. The UHF level calculation provides the ONNO minimum as well (Table 6). However this UHF minimum is much less deep than that of the UMP2 calculation: it is only 0.35 eV below the reactant level and lies high above the product level.

The trans geometry ONNO complex is not presented in the N_2O_2 calculations of ref 23, where only a metastable complex

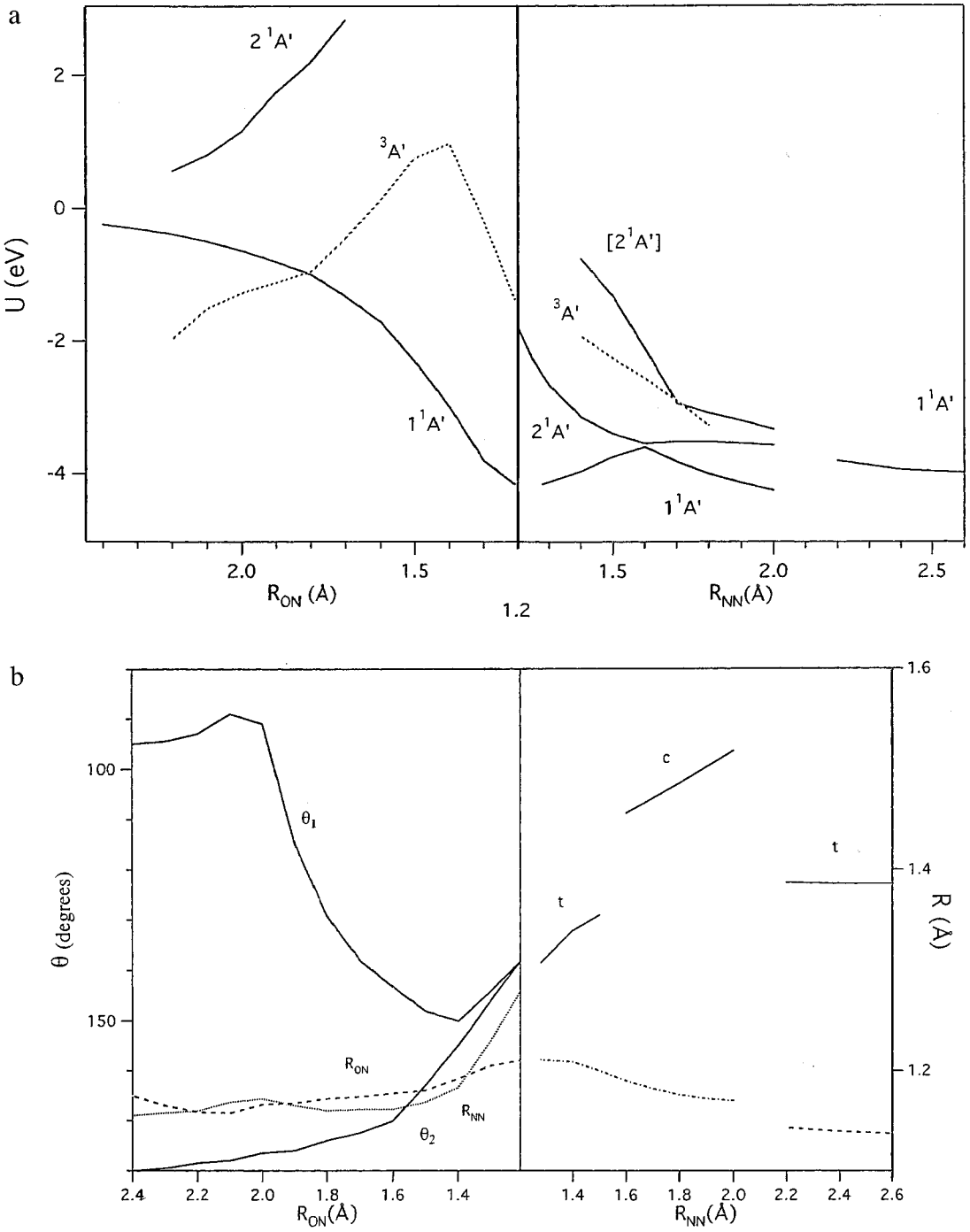

Figure 4. 3D minimum energy path of the reaction $O(^1D) + N_2O \rightarrow 2NO$. (a) Solid line, the lowest $1\ ^1A'$ and the upper $2\ ^1A'$ potentials along their minimum energy paths and the upper $[2\ ^1A']$ potential for the geometry of the lowest $1\ ^1A'$ state. (b) The lowest $1\ ^1A'$ state only. Solid lines, angles (left scale); broken lines, interatomic distances (right scale). The trans and cis geometries are denoted by t and c, respectively. For geometry see Figure 3a.

of a symmetrical cis geometry is described. We have also found this cis geometry complex with almost the same parameters as in ref 23. It lies 2.26 eV below the reactant level, i.e. much higher than the trans geometry ONNO complex. The cis geometry complex is located far from the minimum energy path and consequently is not of much importance for the reaction (1).

The important feature of the reaction dynamics is the preferable approach direction of the incident atom. According to Figure 4b, the minimum energy approach at large $O(^1D)-$NNO distances ($R_{ON} > 1.8$ Å) is almost perpendicular to the NNO line. The $\angle O(^1D)NN$ angle (Figure 3a) of the minimum energy path increases significantly for short distances, but it is still smaller than 150°. The strong deviation of the minimum energy path $\angle O(^1D)NN$ angle from 180° contradicts the assumption that the reaction (1) is preferentially collinear.[5,13] However, due to the high translational energy, the broad interval of the $\angle O(^1D)NN$ angles outside the minimum energy path is expected to be energetically accessible for the system. The PES dependence on the approach $\angle ONN$ angle for fixed NNO geometry parameters R_{NN}, R_{NO}, and $\angle NNO$ (equal to those of the minimum energy path) is shwon in Figure 5. At $R_{ON} = 1.8$ Å the angle dependence is so flat that the meaning of the minimum energy angles is almost lost. At $R_{ON} = 1.4$ Å, which is close to the R_{ON} of the minimum energy configuration (1.21 Å), the $\angle ONN = 180°$ potential (the collinear one) is only 0.23 eV higher than in the minimum energy path point ($\angle ONN = 150°$). Taking into account that in the region of the potential

TABLE 6: Properties of the 3D ONNO and OONN Minima[a]

	ONNO		OONN	
	UHF	UMP2	UHF	UMP2
R_{NN}	1.151	1.279	1.073	1.139
R_{ON}	1.146	1.211	1.198	1.219
R_{OO}			1.722	1.515
∠ONN	108.5°	138.3°	179.4°	179.3°
∠OON			104.1°	103.4°
$-E - 258$	0.498 29	1.379 57	0.428 68	1.272 18
U	−2.242	−4.158	−0.347	−1.236
ν_1	2023	2167	2645	2118
ν_2	1980	1998	1236	1187
ν_3	1061	1393	718	681
ν_4	578	905	672	568
ν_5	499	627	311	511
ν_6	56		201	217

[a] Both ONNO and OONN are in a planar trans configuration in the $^1A'$ state. The ONNO geometry is symmetrical (C_{2h} symmetry) with $R_{NO} = R_{ON}$ and ∠ONN = ∠NNO. The distances R are in Å, frequences ν are in cm^{-1}, total energy E is in au, and potential energy U is in eV. The reactant $O(^1D) + N_2O$ energy is accepted as the U reference level.

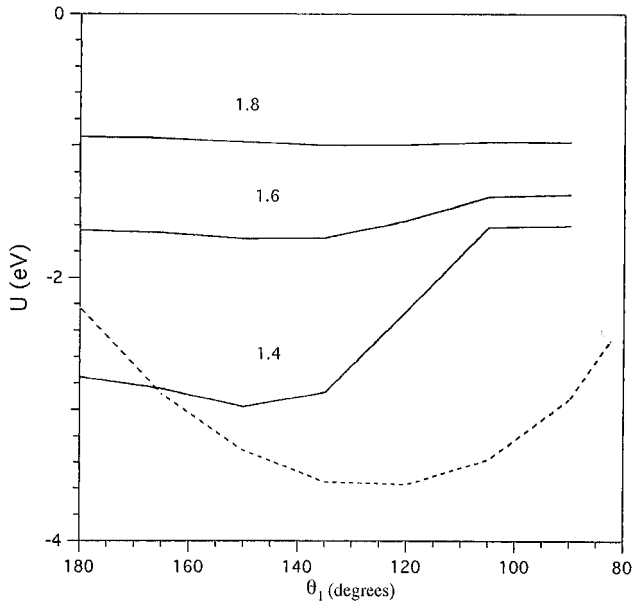

Figure 5. Angular ∠ONN dependence of the ONNO planar PES for frozen NNO geometry of the minimum energy path (Figure 4b). For the system geometry see Figure 3a. Solid lines, entrance valley; the numbers stand for $O(^1D)N$ distances (1.4, 1.6, 1.8 Å). Broken line, saddle point ($R_{NN} = 1.62$ Å, $R_{NO} = R_{NO} = 1.185$ Å, ∠NNO = 1.06°, cis orientation).

well the kinetic energy of colliding particles is high, about 4 eV, the potential difference of 0.23 eV is not of importance. Hence, it is better to speak about the minimum energy angle interval which covers roughly 180° ± 50°. At the perpendicular ∠ONN angle the potential energy is higher by about 1.4 eV than in the minimum point, but it is still negative and consequently accessible for the system. The results presented above show at least that the reaction is not strongly dominated by a collinear collision. It is possible to speak about weakly oriented reaction collision. At large $O(^1D)-N$ distances the NNO fragment geometry is almost collinear, but the ∠NNO angle begins to decrease smoothly when the system is approaching the PES minimum. In the entrance valley the ON fragments are trans oriented.

In the exit valley the system is in a symmetrical geometry ($R_{ON} = R_{NO}$ and θ = ∠ONN = ∠NNO) along the minimum energy path. In the beginning of this valley the θ angle decreases monotonously while the NO fragments are trans oriented. Near the saddle point ($R_{NN} = 1.6$ Å) a discontinuity in the angle behavior is observed when the system becomes more stable in the cis geometry. However at $R_{NN} > 1.6$ Å the potential energy dependence on the angle of the NO rotation around the N−N line is very flat, so that the difference between trans and cis orientation is not of much importance. At $R_{NN} = 1.6$ Å the trans and cis configurations are separated by a small barrier of about 0.3 eV. In the strong interaction region ($R_{ON} \geq 1.4$ Å in the entrance valley and $R_{NN} \leq 1.4$ Å in the exit valley) the cis structure lies roughly 1 eV higher than the trans one. But already at $R_{ON} = 1.6$ Å of the entrance valley the difference between the cis and trans potential energies drops to ∼0.2 eV.

It deserves mentioning that in the asymptotic region of the exit valley vdW ON−NO minima were found. The dissociation energies of these vdW minima are $D_e = 0.035$ eV (trans configuration) and $D_e = 0.021$ eV (cis configuration), whereas the CI calculation provides for the most stable vdW $(NO)_2$ dimer, $D_e = 0.143$ eV (in cis configuration).[21] The empirical value is $D_e = 0.126$ eV. As it was possible to expect, the results of the UMP2 calculation of the vdW complexes are of very low accuracy.

In our discussion we have considered one $^1A'$ state only. However, there are two states of the same symmetry, $1\ ^1A'$ and $2\ ^1A'$, which are degenerate in the reactant and product asymptotes.[1] The two $^1A'$ states demonstrate avoided crossing somewhere between the potential minimum and saddle points. The avoided crossing becomes apparent, in particular, in the electronic structure of the $1\ ^1A'$ state along the minimum energy path. In the entrance valley and in the beginning of the exit valley, up to the saddle point, the occupied orbitals are presented by 13 MOs of A′ symmetry and two MOs of A″ symmetry. After the saddle point the respective numbers are 12 MOs of A′ symmetry and three MOs of A″ symmetry. The upper PES $2\ ^1A'$ is presented in Figure 4a along with the lower $1\ ^1A'$ PES. The $2\ ^1A'$ PES with optimized geometry has in the entrance valley a maximum of about 3 eV, which prevents the reaction channel via the upper $2\ ^1A'$ state. The $2\ ^1A'$ minimum energy path is of cis geometry in the entrance valley and of trans geometry in the exit valley. At $R_{NN} \approx 1.6$ Å of the exit valley the gap between two PESs becomes very narrow, but actually there is no crossing here, as the PESs are in different geometries. When the $2\ ^1A'$ PES in the geometry of the $1\ ^1A'$ state ([$2\ ^1A'$] in Figure 4a) is considered, the gap becomes relatively big, but the typical behavior of avoided crossing is still observed.

As was already mentioned in the Introduction, we are considering the reaction in the singlet state, which is the excited state of the reactants. It may be of some interest to know also the behavior of the triplet $^3A'$ PES, at least along the singlet state minimum energy path (Figure 4a). According to the results presented in Figure 4a, the triplet state potential energy increases sharply in the interaction region of the entrance valley, crossing the singlet state PES at $R_{ON} \approx 1.87$ Å. The triplet state potential energy has a maximum at $R_{ON} \approx 1.43$ Å, where it is about 4 eV over the ground state energy of the reactants.

4.2. $O(^1D) + N_2O \rightarrow O_2(a^1\Delta_g) + N_2$ Reaction. The reaction channel (3) takes place when the singlet state oxygen atom approaches the O atom of the N_2O molecule (Figure 3b). The 3D minimum energy path of this reaction channel (Figure 6) has been produced by the UMP2 level calculation, like in the previous case. It was found to lie in a planar geometry (except for a narrow interval in the exit valley) and to belong to the $^1A'$ state. The minimum energy path presented in Figure 6a demonstrates a minimum in the entrance valley and a saddle point in the exit valley. However, unlike the previous reaction

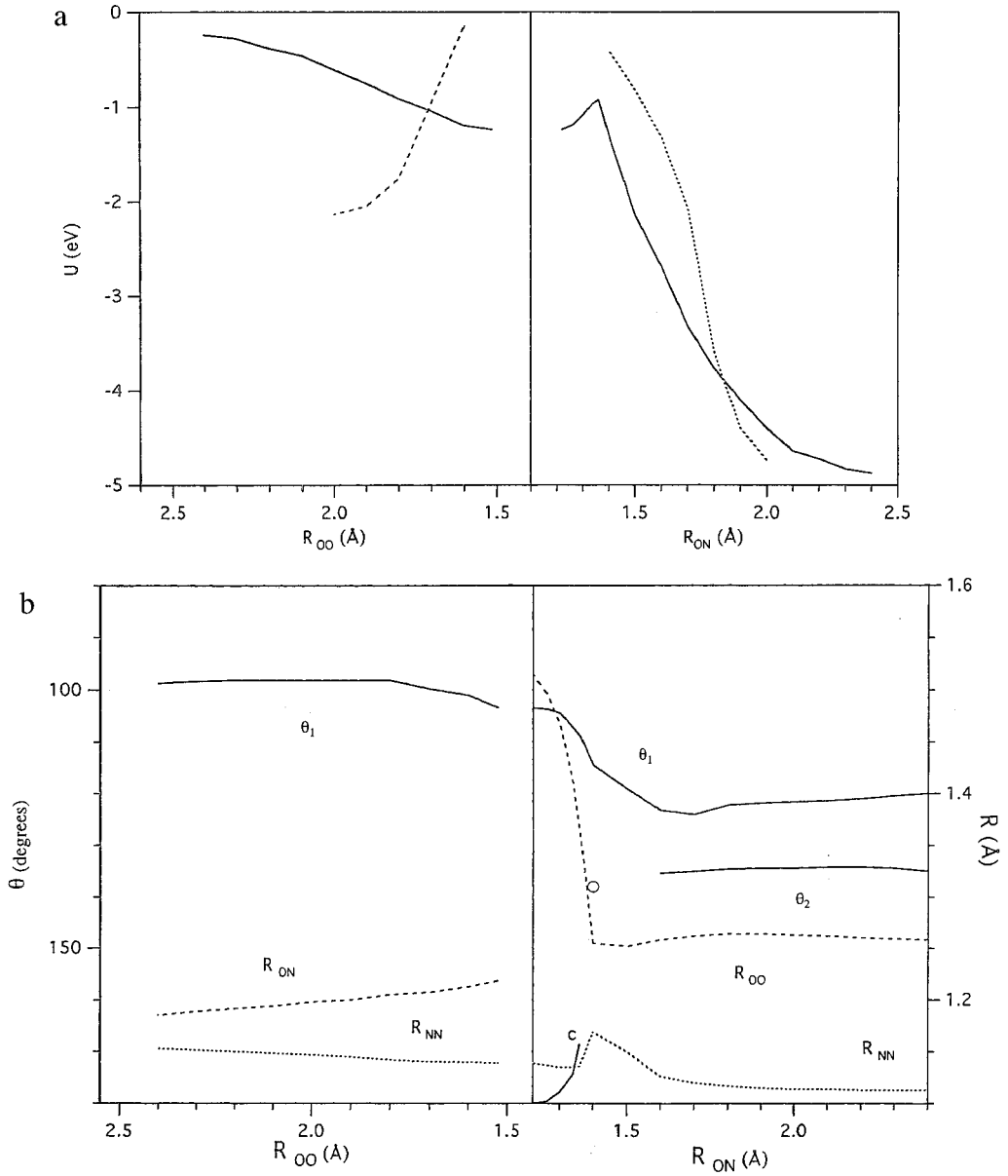

Figure 6. 3D minimum energy path of the reaction $O(^1D) + N_2O \rightarrow O_2(a\ ^1\Delta_g) + N_2$ in the lowest $^1A'$ state. For notations see Figure 4. For geometry see Figure 3b. The out-of-planar point is denoted in part b by a circle.

channel (Figure 4a), the potential minimum is shallow. The parameters of the planar OONN minimum are presented in Table 6. These parameters are close to those of the metastable α-N_2O_2 isomer of ref 23. The OONN metastable isomer consists of a slightly deformed and almost collinear ONN molecule and the (O^1D) atom attached to the O end of the ONN molecule. The $\angle$OON angle of the OONN metastable isomer is a little bigger than 90°. The zero vibrational energy is 0.327 eV.

The OONN potential minimum lies 1.24 eV below the reactant level and some 3.7 eV over the product level. It follows that the main portion of the potential energy release is realized in the exit valley, after the system passes the saddle point. The saddle point potential energy is low, only 0.31 eV above the potential minimum. The saddle point lies about 1 eV below the reactant level, so it is energetically accessible. The metastable OONN potential minimum found in our calculation cannot be considered as a long living complex since the system is expected to overcome easily the low saddle point. The UHF level calculation provides also a metastable configuration whose potential energy lies only 0.35 eV below the reactant level (Table 6). The geometry of the UHF minimum differs, however, little from the UMP2 geometry.

The approaching $O(^1D)$ atom does not affect much the N_2O molecule along the minimumm energy path of the entrance valley. Up to the minimum energy point the ONN molecule remains practically linear and its NN distance is almost frozen. Only the ON distance is slightly increasing (Figure 6b). The direction of the $O(^1D)$ minimum energy approach to the ONN molecule is close to the perpendicular one, in qualitative agreement with the UHF results of ref 15. Taking into account the purely repulsive character of the collinear $O(^1D)$ + OON interaction (Figure 2), it is possible to conclude that the reaction (3) is of strongly noncollinear character. In the interaction region of the entrance valley the potential energy is negative in a relatively wide interval of the $\angle$OON angles. These intervals are 67−170° and 68−180° for $R_{OO} = 1.6$ and 1.8 Å, respetively (Figure 7).

In the beginning of the exit valley the OONN geometry is changing drastically. At the saddle point ($R_{ON} = 1.36$ Å) the ONN geometry is already strongly deformed with a $\angle$ONN angle of about 170°. The saddle point potential dependence on the $\angle$OON angle (for a frozen ONN geometry) is relatively flat for $\angle$OON > 80° (Figure 7). When the $\angle$OON angle becomes smaller than 80°, the potential is increasing sharply,

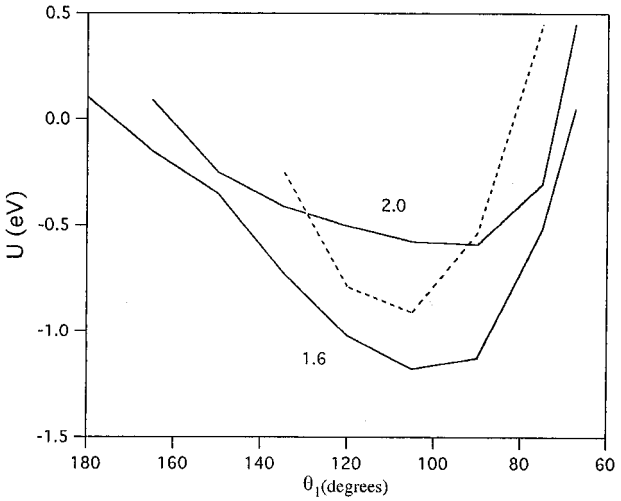

Figure 7. Angular ∠OON dependence of the OONN planar PES for frozen ONN geometry of the minimum energy path (Figure 6b). For the system geometry see Figure 3b. Solid lines, entrance valley; the numbers stand for O(1D)O distances (1.8, 2.0 Å). Broken line, saddle point (R_{ON} = 1.35 Å, R_{OO} = 1.36 Å, R_{NN} = 1.14 Å, ∠ONN = 169°).

which indicates that the forces between the O(1D) atom and the central N atom are repulsive. The OONN geometry is planar and cis oriented in the exit valley for R_{ON} < 1.4 Å. At R_{ON} = 1.4 Å the minimum energy geometry becomes nonplanar since in the vicinity of this point the NN fragment is rotating around the ON line. Beginning from the next point (R_{ON} = 1.6 Å) and up to the asymptotic region the system is trans oriented with almost parallel O_2 and N_2 fragments. The transition to the trans orientation is followed by a strong decrease of the OO distance, which practically reaches the O_2(a $^1\Delta_g$) equilibrium distance at $R_{ON} \approx$ 1.6 Å.

In the entrance valley, due to the almost collinear ONN geometry, the mutual orientation of the terminal OO and NN bonds is not of any importance. It becomes of some importance only in the vicinity of the saddle point. Thus at R_{ON} = 1.4 Å the potential energy is about 0.4 eV higher in the cis geometry than in the minimum energy (nonplanar) geometry. The potential energy dependence on the mutual OO and NN orientation becomes flat again for R_{ON} > 1.6 Å. Like in the case of the reaction (1), the saddle point is widely open (Figure 7) and is not expected to affect much the reaction.

At a large O_2(a $^1\Delta_g$)−N_2 separation ($R_{ON} \approx$ 3.04 Å) a vdW complex was found with a small dissociation energy of D_e = 0.022 eV. However, as was mentioned above, the accuracy of the UMP2 calculation of a vdW complex is low. Any other O_2(a $^1\Delta_g$)−N_2 vdW complex calculations are unknown to us.

As was discussed already in the Introduction, the spin-forbidden reaction (2) consists most probably of two steps, the first one being the single state reaction (3), whose PES is treated here. In the second step the excited single state oxygen molecule O_2(a $^1\Delta_g$) is deactivated to the ground state triplet molecule O_2(X $^3\Sigma_g^-$). Another possibility, which looks much less feasible, is the direct nonadiabatic transition from the single state to the triplet one. To obtain some idea about the possibility of this nonadiabatic transition, we performed the PES calculation of the triplet state asymptotic to the ground state of the reactant and product molecules. The results of this calculation for the geometry of the single state ^{1}A′ minimum energy path are shown in Figure 6a. In the entrance valley there is a crossing of the singlet and triplet PESs at an almost perpendicular angle, which makes the nonadiabatic transition probability negligibly small.[30] The second crossing takes place in the exit valley, where the nonadiabatic transition to the triplet state is, generally speaking, possible, although the probability of such a transition is expected to be small. In the regions located far away from the ^{1}A′ minimum energy path other crossings may be present, but these regions are not supposed to be accessible for the ^{1}A′ trajectories, at least at low collision energies.

5. Model Potential of the O(1D) + N2O → 2NO, O2(a 1Δg) + N2 Reaction Channels

To perform a dynamical study by quasiclassical trajectories of the O(1D) + N_2O reaction channels, one needs an analytical representation of the N_2O_2 PES. The most straightforward way to get an analytical representation of a PES is provided by the procedure of an analytical fitting of a known *ab initio* PES. The fitting procedure presents a difficult task even in the case of simple three-atomic systems. It is a much more difficult task, obviously, to fit the *ab initio* PES of a complicated four-atomic system such as N_2O_2. However, in addition to the problem of the N_2O_2 PES complexity, the fitting procedure presents another problem, which results from a relatively low accuracy of the *ab initio* UMP2 calculations. When a direct fitting is performed, the analytical potential consequently incorporates the errors of the *ab initio* calculation. It is impossible to estimate these errors in the interaction region, but they are well-known in the asymptotic regions, where the calculated and experimental parameters of the reactant and product species can be compared with one another (Tables 2−4). According to Tables 2 and 3, the calculated dissociation energies differ significantly from the experimental values. For example, the $N_2O \rightarrow N_2 + O(^1D)$ dissociation energy, D_e, of the UMP2 calculation is by 1.19 eV larger than the experimental D_e (Table 3). The differences between the UMP2 and experimental exoergicities of reactions (1) and (3) are about 0.5 eV (Table 4). It seems unreasonable to follow the nonaccurate UMP2 potentials of the asymptotic regions, while the experimental potentials are at our disposal.

Taking into account the reasons presented above, we decided not to perform the procedure of the analytical fitting. As an alternative solution for the problem of the analytical representation of the N_2O_2 PES, we suggested constructing a model analytical potential that describes by experimental parameters the reactant and product species and follows roughly the main features of the calculated UMP2 PES in the interaction region. By the main features of the PES we mean the regions of potential descent, potential minima, saddle points, minimum energy approach angles, angle dependence outside the minimum energy path, and some others. The *ab initio* potential of the interaction region has to be calibrated to be consistent with the experimental potentials of the asymptotic regions. Some examples of this kind of calibration will be presented later.

The N_2O_2 model potential U that meets the conditions discussed above has been found by trying various analytical expressions. The final version of the N_2O_2 model potential is presented as the following sum of diatomic and multicenter terms:

$$U = W_{NO}(1) + W_{NO}(6) + W_{NN}(4) + W_{OO}(3) + V_1(2) + V_2(2) + P(5) + E_D Q(1,3,4,6) + H_c(2,3,4,5,6) + H_a(1,3,5) \quad (4)$$

where the argument numbers indicate the interatomic fragments (Figure 8). In eq 4 W are Morse potentials, V are Gaussian functions, P is an exponential function, and E_D = 1.968 eV is the experimental value of the excited oxygen atom O(1D) energy. The Q term is expressed by diatomic Gaussian functions and becomes 1 for reactants (separated O(1D) + N_2O)

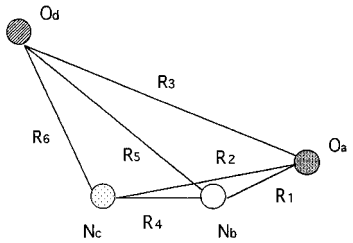

Figure 8. N_2O_2 geometry designations of the model potential (4). The numbers indicate the diatomic fragments of the system. The reactant $O(^1D)$ atom is denoted by O_d, another O atom is denoted by O_a. The terminal N atom of the reactant N_2O molecule is denoted by N_c; another N atom is denoted by N_b.

TABLE 7: Properties of the ONNO and OONN Minima of the Analytical Model Potential[a]

ONNO		OONN	
R_{ON}	1.195	R_{OO}	1.305
R_{NN}	1.177	R_{ON}	1.277
R_{NO}	1.201	R_{NN}	1.133
∠ONN	142.6°	∠OON	97.8°
∠NNO	167.2°	∠ONN	176.4°
config.	trans	config.	cis
U	−3.505	U	−1.231

[a] The geometry is planar. The distances R are in Å; the potential energy U is in eV. The reactant $O(^1D) + N_2O$ energy is accepted as the U reference level.

and 0 for products of both reaction channels. The H terms are expressed in a relatively complicated way by Gaussian (F) and cosine (Φ) functions and becomes 0 in both reactant and product asymptotics.

$$H_c(R_2,R_3,R_4,R_5,R_6) = [S_c + \Phi^2(R_4,R_6;R_5) - \Phi^2(R_2,R_6;R_3)]F_c(R_4,R_6) \quad (5)$$

$$H_a(R_1,R_3,R_5) = [S_a + \Phi^2(R_1,R_3;R_5)]F_a(R_1,R_3) \quad (5')$$

For the expressions of terms in eqs 4 and 5 see the Appendix.

In the reactant asymptotic geometry the model potential becomes equal to the sum of the $O(^1D)$ excitation energy, E_D, and the atomization energy of the N_2O molecule. The last one, according to eq 4, is expressed in the following way:

$$E[N_2O] = W_{NO}(1) + W_{NN}(4) + V_1(2) + V_2(2) \quad (6)$$

The parameters of the Gaussian fucntios V_1 and V_2 were used to fit the atomization energy (exactly) and the experimental geometry (approximately) of the N_2O molecule. In the product asymptotics the model potential becomes equal to the sum of the corresponding Morse potentials.

In the model potential (4) the two O atoms are presented in a nonidentical way; that is, the reactant $O(^1D)$ atom, O_d, interacts in a different way than the O_a atom of the reactant N_2O (Figure 8). Due to this difference, the ONNO PES minimum of the reaction channel (1) is not symmetric, contrary to the UMP2 PES (Table 6), but the deviations from the symmetrical geometry are small. The nonidentical presentation of the O atoms may result in an unphysical change in the system energy when these atoms are exchanged. However the O atoms exchange channel is not of interest because of a high barrier.

The problem of the *ab initio* potential calibration is well demonstrated for the case of the ONNO and OONN minima (Table 7). In the UMP2 calculation the depth of the ONNO minimum (4.16 eV, Table 6) is a little bit larger than the reaction (1) exoergicity (3.97 eV, Table 4). Taking into account that this depth is probably overestimated (see the discussion in section 4.1), we suggested that the model potential ONNO minimum depth has to be close to the experimental exoergicity, which is equal to 3.50 eV (Table 4). The depth of the reaction channel (3) OONN minimum was found to be much smaller than the exoergicity (Tables 4, 6), so we decided to accept the UMP2 value of 1.23 eV for the model potential (Table 7).

In the vincinity of the minimum energy paths the model potential fits roughly the UMP2 potential angle dependence (see Figures 5 and 7). In the configuration regions located far away from the minimum energy paths we do not have any UMP2 points to be used for the model potential construction. In these regions, however, the PES is expected to lie relatively high, so that the details of its structure are not of much interest, at least for low collision energies. The model potential (4) in these regions is really high, and it is changing smoothly without demonstrating any unreasonable features.

5. Conclusions

1. To treat the PESs of the reaction channels (1) and (3), the *ab initio* MP calculations of the N_2O_2 system and its components have been performed. The *ab initio* calculations of the NO, N_2, $O_2(a\ ^1\Delta_g)$, and N_2O molecules and the PESs of the collinear ONNO and OONN reactive systems show that the UMP4 level results do not differ much from those obtained at the UMP2 level. Taking this into account, it was decided to apply the much less time consuming UMP2 level to the 3D PES calculation of the N_2O_2 system.

2. According to the 3D UMP2 level calculation, the minimum energy path of the reaction channel (1) lies in a planar geometry and belongs to the $^1A'$ state. The minimum energy path does not demonstrate any reaction barrier. In the entrance valley it has a minimum having symmetrical geometry with a trans orientation of the terminal ON and NO bonds. Due to this minimum, most of the energy is released in the entrance valley. The minimum energy approach of $O(^1D)$ to N_2O is far from collinear, but since the PES angle dependence is flat, the reaction is weakly oriented. In addition to the lower (reactive) $^1A'$ PES, there is also a higher $^1A'$ PES. In the exit valley the two $^1A'$ PESs demonstrates an avoided crossing.

3. According to the 3D UMP2 level calculation the minimum energy path of the reaction channel (3) lies in a planar geometry and belongs to the $^1A'$ state, except for a very narrow region in the exit valley, where the terminal bonds OO and NN are rotating out of a planar geometry, changing the configuration from cis to trans. The minimum energy path has a shallow well in the entrance valley. The main portion of the energy is released in the exit valley. In the entrance valley the minimum energy approach of the $O(^1D)$ atom is almost perpendicular to the ONN molecule, which remains practically collinear. In the exit valley there is a crossing between the reactive singlet state PES and the lowest triplet state PES, which makes possible the nonadiabatic transition to the ground state products $O_2 + N_2$, although the probability of such a transition is expected to be low.

4. The analytical model potential for the reaction channels (1) and (3) has been constructed. The model potential describes the reactant and product molecules by their experimental parameters. In the interaction region the model potential follows roughly the main features of the calculated UMP2 PES. This analytical model potential will be used in a quasiclassical trajectory study of the $O(^1D) + N_2O$ reaction dynamics, and work in this direction is in progress.

Acknowledgment. We would like to acknowledge Professor J. Jortner for valuable discussions. This work has been

supported by the "Dirección General de Investigación Científica y Técnica" of the Spanish Ministry of Science and Education (DGICYT Project Numbers PB 92-0756 and SAB 94-0201) and by the "Generalitat de Catalunya" (CUR.DGU Project GRQ02121). I.L. thanks Barcelona University for its hospitality during a visit in 1994−1995 when this work was performed.

Appendix

The Appendix presents the terms in eqs 4 and 5.

$W(R)$ terms are the Morse function that describe the diatomic fragments NO, NN, and OO.

$$W(R) = D_e G(G - 2) \quad \text{(A.1)}$$

$$G(R) = \exp[-\alpha(R - r)] \quad \text{(A.2)}$$

NO: $D_e = 6.615$ eV, $\alpha = 2.75$ Å^{-1}; $r = 1.151$ Å

NN: $D_e = 9.905$ eV, $\alpha = 2.7$ Å^{-1}, $r = 1.098$ Å

OO: $D_e = 4.308$ eV, $\alpha = 2.82$ Å^{-1}, $r = 1.251$ Å

The OO parameters differ slightly from the experimental values (Table 2) in order to fit better the *ab initio* PES of the reaction channel (3).

$V(R)$ terms are Gaussian functions.

$$V(R) = B \exp[-\beta(R - \delta)^2] \quad \text{(A.3)}$$

V_1: $B = 5.0$ eV, $\beta = 1.6$ Å^{-2}, $\delta = 2.1$ Å

V_a: $B = 65.0$ eV, $\beta = 1.3$ Å^{-1}, $\delta = 0$

$P(R)$ is a repulsive exponential function.

$$P(R) = A \exp[-\alpha R] \quad \text{(A.4)}$$

$$A = 180 \text{ eV}, \alpha = 3.4 \text{ Å}^{-1}$$

The multicenter Q term is expressed by Gaussian functions.

$$Q(R_6,R_4,R_3,R_1) = 1 + G_6(R_6)[G_4(R_4) - 1] + G_3(R_3)[G_1(R_1) - 1] \quad \text{(A.5)}$$

$$G_k(R_k) = \exp[-\gamma_k(R_k - \rho_k)^2] \quad \text{(A.6)}$$

$\gamma_6 = 1.0$ Å^{-2}, $\rho_6 = 1.0$ Å; $\gamma_4 = 0.5$ Å^{-2}; $\rho_4 = 1.151$ Å;
$\gamma_3 = 0.8$ Å^{-2}, $\rho_3 = 1.2$ Å; $\gamma_1 = 0.5$ Å^{-2}, $\rho_1 = 1.215$ Å

The Gaussian and cosine functions of the multicenter terms H_c and H_a are as follows:

$$F(R_i,R_j) = B \exp[-\beta(R_i + R_j - r)^2] \quad \text{(A.7)}$$

$$\Phi(R_i,R_j,R_k) = (R_i^2 + R_j^2 - R_k^2)/2R_iR_j \quad \text{(A.8)}$$

H_c: $S_c = 2.0$ eV, $B = 2.15$ eV, $\beta = 1.1$ Å^{-2}; $r = 1.8$ Å

H_b: $S_a = 2.0$ eV, $B = 1.62$ eV, $\beta = 1.2$ Å^{-2}, $r = 2.2$ Å

References and Notes

(1) Donovan, R. J.; Husain, D. *Chem. Rev.* **1970**, *70*, 489.
(2) Wiesenfeld, J. R. *Chem. Phys. Lett.* **1977**, *45*, 384.
(3) Levy, M. R. *Prog. React. Kinet.* **1979**, *10*, 1.
(4) Davidson, J. A.; Howard, C. J.; Schiff, H. I.; Fehsenfeld, F. C. *J. Chem. Phys.* **1979**, *70*, 1697.
(5) Ben-Nun, M.; Brouard, M.; Simons, J. P.; Levine, R. D. *Chem. Phys. Lett.* **1993**, *210*, 423.
(6) Atkinson, R.; Baulch, D. L.; Cox, R. A.; Hampson, R. F., Jr.; Kerr, J. A.; Froe, J. *J. Phys. Chem. Ref. Data* **1992**, *21*, 1125.
(7) Paraskevopoulos, G.; Cvetanovic, R. J. *J. Chem. Phys.* **1969**, *50*, 590.
(8) Preston, K. F.; Barr, R. F. *J. Chem. Phys.* **1971**, *54*, 3347.
(9) Felder, P.; Haas, B.-M.; Huber, J. R. *Chem. Phys. Lett.* **1991**, *186*. 177.
(10) Boxall, C. R.; Simons, J. P.; Tasker, P. W. *Faraday Discuss. Chem. Soc.* **1972**, *53*, 182.
(11) Chamberlain, G. A.; Simons, J. P. *J. Chem. Soc., Faraday Trans 2* **1975**, *71*, 402.
(12) Brouard, M.; Duxon, S. P.; Enriquez, P. A.; Sayos, R.; Simons, J. P. *J. Phys. Chem.* **1991**, *95*, 8169.
(13) Brouard, M.; Duxon, S. P.; Enriquez, P. A.; Simons, J. P. *J. Chem. Phys.* **1992**, *97*, 7414.
(14) Honma, K.; Kajimoto, O. *Chem. Phys. Lett.* **1985**, *117*, 123.
(15) Honma, K.; Fujimura, Y.; Kajimoto, O.; Inoue, G. *J. Chem. Phys.* **1988**, *88*, 4739.
(16) Goldstein, N.; Greenblatt, G. D.; Wiesenfeld, J. R. *Chem. Phys. Lett.* **1983**, *96*, 410.
(17) Overend, R.; Paraskevopoules, G.; Crawford, J. R.; Wiebe, H. A. *Can. J. Chem.* **1975**, *53*, 1915.
(18) Wong, A. T.; Bacskay, G. B. *Chem. Phys. Lett.* **1993**, *207*, 360.
(19) Foo, P. D.; Lohman, T.; Podolske, J.; Wiesenfeld, J. R. *J. Phys. Chem.* **1975**, *79*, 414.
(20) Saxon, R. P.; Liu, B. *J. Chem. Phys.* **1977**, *67* 5432.
(21) Gonzalez-Luque, R.; Merchan, M.; Roos, B. O. *Theor. Chim. Acta* **1994**, *8*, 425.
(22) (a) Michels, H. H.; Montgomery, J. A. *J. Chem. Phys.* **1988**, *88*, 7248 (b) Nguyen, K. A.; Gordon, M. S.; Montgomery, A., Jr.; MIchels, H. H.; Yarkony, D. *J. Chem. Phys.* **1993**, *98*, 3845 (c) Nguyen, K. A.; Gordon, M. S.; Boatz, J. A. *J. Am. Chem. Soc.* **1994**, *116*, 9241 (d) Arnold, D. W.; Neumark, D. M. *J. Chem. Phys.* **1995**, *102*, 7035.
(23) Nguen, K. A.; Gordon, M. S.; Montgomery, J. A.; Michels, H. H. *J. Phys. Chem.* **1994**, *98*, 10072.
(24) Frish, M. J.; Trucks, G. W.; Head-Gordon, M.; Gill, P. M. W.; Wong, M. W.; Foresman, J. B.; Johnson, B. G.; Schlegel, H. B.; Robb, M. A.; Replogle, E. S.; Gomperts, R.; Andres, J. L.; Raghavachari, K.; Binkley, J. S.; Gonzalez, C.; Martin, R. L.; Fox, D. J.; Defrees, D. J.; Baker, J.; Stewart, J. J. P.; Pople, J. A. *GUASSIAN-92*, Revision D2; Gaussian, Inc.: Pittsburgh, Pa, 1992.
(25) Walch, S. P.; Jaffe, R. L. *J. Chem. Phys.* **1987**, *86*, 6946.
(26) Siegbahn, P. E. M. *Int. J. Quantum Chem.* **1983**, *23*, 1869.
(27) Teffo, J.-L.; Chèdin, A. *J. Mol. Spectrosc.* **1989**, *135*, 389.
(28) Hopper, D. G. *J. Chem. Phys.* **1984**, *80*, 4290.
(29) (a) Goumri, A.; Rocha, J.-D. R.; Laakso, D.; Smith, C. E.; Marshall, P. *J. Chem. Phys.* **1994**, *101*, 9405 (b) Yamaguchi, K.; Jensen, F.; Dorigo, A.; Houk, K. N. *Chem. Phys. Lett.* **1988**, *149*, 537.
(30) Tully, J. C.; Preston, R. K. *J. Chem. Phys.* **1971**, *55*, 562.